Stochastic heating of a single Brownian particle by charge fluctuations in a radio-frequency produced plasma sheath

Christian Schmidt* and Alexander Piel†
IEAP, Christian-Albrecht-Universität, D-24098 Kiel, Germany
(Received 23 July 2015; revised manuscript received 30 September 2015; published 19 October 2015)

The Brownian motion of a single particle in the plasma sheath is studied to separate the effect of stochastic heating by charge fluctuations from heating by collective effects. By measuring the particle velocities in the ballistic regime and by carefully determining the particle mass from the Epstein drag it is shown that for a pressure of 10 Pa, which is typical of many experiments, the proper kinetic temperature of the Brownian particle remains close to the gas temperature and rises only slightly with particle size. This weak effect is confirmed by a detailed model for charging and charge fluctuations in the sheath. A substantial temperature rise is found for decreasing pressure, which approximately shows the expected scaling with p^{-2}. The system under study is an example for non-equilibrium Brownian motion under the influence of white noise without corresponding dissipation.

DOI: 10.1103/PhysRevE.92.043106 PACS number(s): 52.27.Lw, 05.40.Jc, 52.25.Gj

I. INTRODUCTION

The Brownian motion of a single micrometer-sized particle has attracted much attention in the last few years. The transition from diffusive to ballistic motion was studied by means of optical tweezers in gases [1] and in liquids [2,3]. By absorption of laser light, the Brownian particle can attain a high surface temperature, which leads to "hot Brownian motion" [4–6]. This is an interesting case for non-equilibrium Langevin dynamics, in which the Brownian particle is in simultaneous contact with two heat baths of cold incoming and hot outgoing gas atoms.

A further interesting situation for non-equilibrium stochastic motion is found in "complex" plasmas. Microparticles in a plasma environment were often found to possess extremely high kinetic temperatures, which reached 20–300 eV in current-carrying particle clouds [7] or several ten eV in multilayer particle clouds [8,9]. Only in two-dimensional systems moderate temperatures of 390–1240 K were found in monolayers [10] and 370–2890 K in small two-dimensional clusters [11], which still substantially exceed the temperature of the neutral gas (≈300 K) in which the microparticles are embedded. For a pair of MF particles of $r_p = 2.4\,\mu$m confined in a 1D trap at $p = 1.8$ Pa an enhanced temperature of 430 K was reported recently [12,13].

The present state of understanding is that the excessive temperatures in the 10–100 eV range are attributed to plasma-induced instabilities of the microparticle system [14–16], while the less violent heating mechanism is ascribed to stochastic heating from charge fluctuations [17–19]. However, neither this distinction into the two classes of unrelated phenomena has been experimentally verified nor has the stochastic heating by charge fluctuations been clearly separated from collective phenomena in experimental situations. Therefore, the primary goal of the present article is to study the Brownian dynamics of an isolated microparticle in the absence of any collective effects that are introduced by other microparticles. In addition, the model for heating by charge fluctuations is scrutinized and all relevant parameters are determined from particle-in-cell simulations of the plasma discharge. The interplay of the Brownian motion of a microparticle in its gas environment with an additional stochastic process is also interesting in itself, because it involves the transition from Langevin dynamics at equilibrium to a non-equilibrium situation.

II. EXPERIMENTAL DETAILS

For studying the Brownian dynamics we have designed an experiment in which a single microparticle is suspended in the sheath of a radio-frequency (r.f.) produced plasma (Fig. 1) with an electrode gap of $d = 30$ mm width and 80 mm electrode diameter. The sheath is a space-charge region with a vertical electric field that is strong enough to levitate the negatively charged microparticle according to the *Millikan condition*

$$q_p \bar{E}_0 = m_p g \ . \tag{1}$$

Here, q_p and m_p are the charge and mass of the microparticle and g the gravitational acceleration. The gradient of the time-averaged electric field $\bar{E}_0$ and the smallness of the vertical excursions provide a nearly harmonic vertical potential trap with an eigenfrequency ω_0 [20]. In the center of the r.f. powered electrode a small manipulation electrode is inserted [21] that can be biased with a positive voltage and serves to deform the time-average potential contour (dashed line) to provide horizontal confinement.

The particle motion is observed side-on with a high-speed video camera (Mikrotron EoSens MC1362) that records a 2× enlarged image covering 80 × 100 pixels corresponding to 526 × 657 μm^2 region in real space. The maximum frame rate is 4000 fps but typically 400 fps are used. A time-series comprises 10^5 frames. In each frame, the particle position is determined with subpixel resolution from the intensity distribution in the particle image, which fills approximately 4 × 4 pixels. For the automatic determination of particle positions we use an algorithm that originates from [22], which uses a suitable threshold value, blurring of the image by a Gaussian filter and determines the "center-of-mass" for this blurred intensity distribution. The plasma chamber and the camera are mounted on an air suspension vibration-isolation table.

*schmidt@physik.uni-kiel.de
†piel@physik.uni-kiel.de

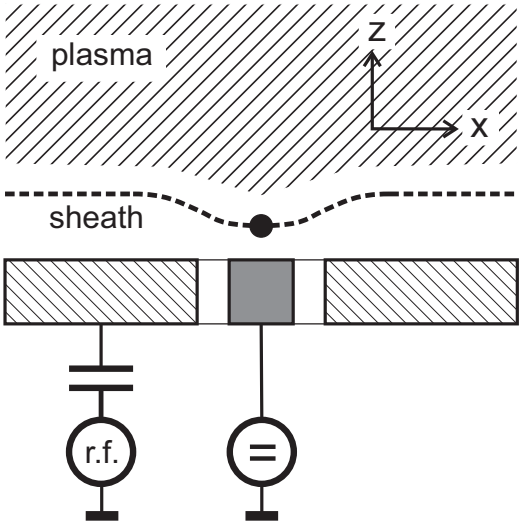

FIG. 1. Sketch of the particle confinement in the sheath of an r.f. parallel plate discharge. The equipotential (dashed line) is deformed by a positive bias on the central manipulation electrode to provide horizontal confinement.

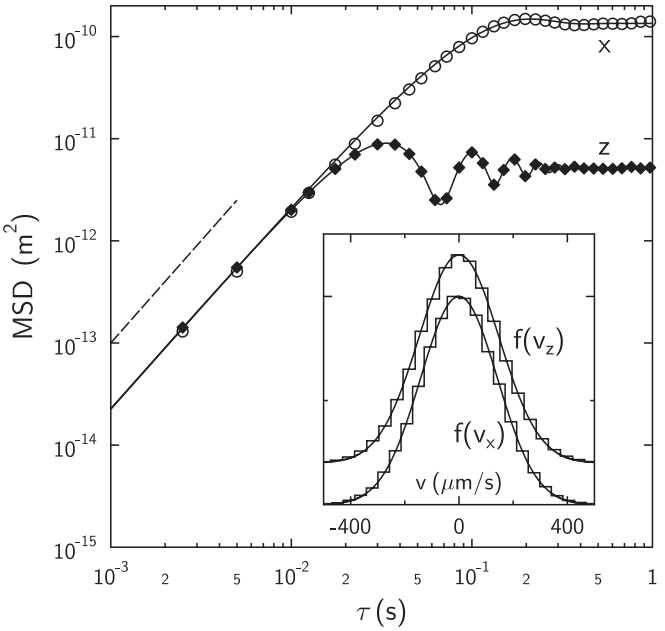

FIG. 2. Mean-squared displacement in x and z directions as a function of the delay time τ. The dashed solid line of slope 2 marks the ballistic regime, which covers the time scales $\tau = (1\text{–}5)$ ms. The inset shows the comparison of the area-normalized velocity distributions $f(v_x)$ and $f(v_z)$ with best-fit Gaussians.

For the present experiments we have primarily chosen monodisperse spherical silica particles, which are non-porous and have a well-specified mass density of $\rho_p = (1850 \pm 93)\,\mathrm{kg\,m^{-3}}$ [23]. These particles are available with radii up to $3.69\,\mu$m. Larger silica particles are porous and have a less well-defined mass density. This maximum size limits our experiments with silica particles. The silica particles are dried at 230 °C for 2 h.

Additional measurements were made with melamine-formaldehyde (MF) particles. MF particles are less suited for these experiments because of their poor long-time stability, which leads to a change in density [24] and a diminishing radius [25]. The stability of the particles is improved by drying at 130 °C for 2 h, which leads to a a reduced density $\rho_p \approx 1440\ \mathrm{kg\,m^{-3}}$ (as estimated from Ref. [24]) compared to 1540 kg $\mathrm{m^{-3}}$ stated by the manufacturer [23]. The discharge conditions were $U_{rf} = 80\,\mathrm{V}_{pp}$ and $p = 10.2\,\mathrm{Pa}$ (argon) for silica particles and $70\,\mathrm{V}_{pp}$, 11 Pa for MF particles.

III. TEMPERATURE MEASUREMENTS

The determination of the proper kinetic temperature of the microparticle requires two independent informations. First, we need proper particle velocities. For this purpose the ballistic regime of particle motion [1] is determined in the plot of the mean-squared displacement (MSD) for an MF-particle with a true radius $r_p = 2.89\,\mu$m shown in Fig. 2. The MSD of a Brownian particle at temperature T in a parabolic trap with eigenfrequency ω_0 is given by [1,26,27]

$$\langle[\Delta x(\tau)]^2\rangle = \frac{2k_BT}{m_p\omega_0^2}\left[1 - \exp\left(-\frac{\beta\tau}{2}\right) \times\left(\cos\omega_1\tau + \frac{\beta}{2\omega_1}\sin\omega_1\tau\right)\right]. \quad (2)$$

Here, $\omega_1^2 = \omega_0^2 - (\beta/2)^2$. The ballistic regime is defined by the scaling $\langle[\Delta x(\tau)]^2\rangle \propto \tau^2$. The frame rate of the video recordings is chosen as 400 fps ($\tau = 2.5$ ms), which defines the time step for calculating $\langle v^2\rangle$. The proper choice of the frame rate is discussed in more detail in the Appendix.

The fit of the Uhlenbeck-Ornstein model (2) to the measured MSD-curve further yields the eigenfrequencies $\omega_x = 18.1\,\mathrm{s^{-1}}$ and $\omega_z = 94.0\,\mathrm{s^{-1}}$ for the horizontal and vertical trap, as well as the friction coefficients $\beta_x = 20.1\,\mathrm{s^{-1}}$ and $\beta_z = 16.8\,\mathrm{s^{-1}}$. The difference between the two friction coefficients is attributed to the low accuracy of extracting β_x from the MSD. The velocity distribution shown in the inset of Fig. 2 is found very close to a Maxwellian.

Second, we need to find the proper mass of the particles. This is done by measuring the Epstein friction coefficient β with a method that is more accurate than the MSD fit. For this purpose we use the velocity autocorrelation function (VAF), which for a particle in a harmonic trap has the shape [27]

$$\langle v(t)v(t+\tau)\rangle = \frac{k_BT}{m_p}\exp\left(-\frac{\beta\tau}{2}\right)\left(\cos\omega_1 t - \frac{\beta}{2\omega_1}\sin\omega_1 t\right). \quad (3)$$

The particle radius r_p is related to the friction coefficient by [28]

$$\beta = \delta\frac{8p}{\pi r_p\rho_m v_{th}} \quad (4)$$

with the coefficient for diffuse reflection $\delta = 1.44$ [29], gas pressure p, and gas thermal velocity v_{th}. The close agreement of the measured normalized VAF with Eq. (3) in Fig. 3 shows that the VAF provides a sensitive method for determining β.

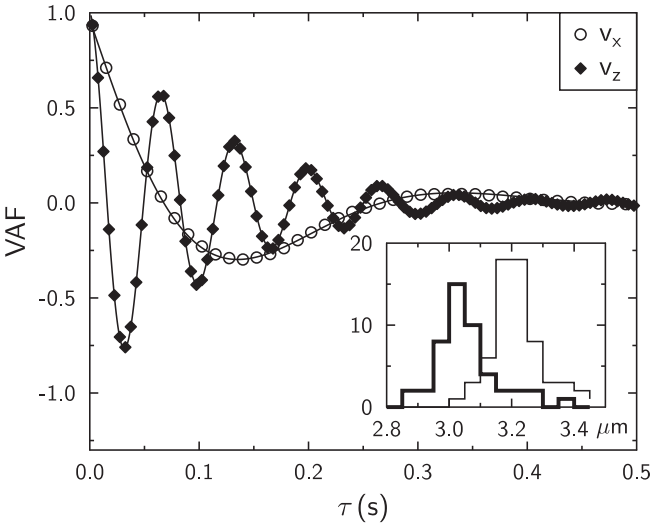

FIG. 3. Measured normalized velocity autocorrelation functions for x and z directions in comparison with Eq. (3). The inset shows the distribution of MF particle radii before (light line) and after drying (heavy line).

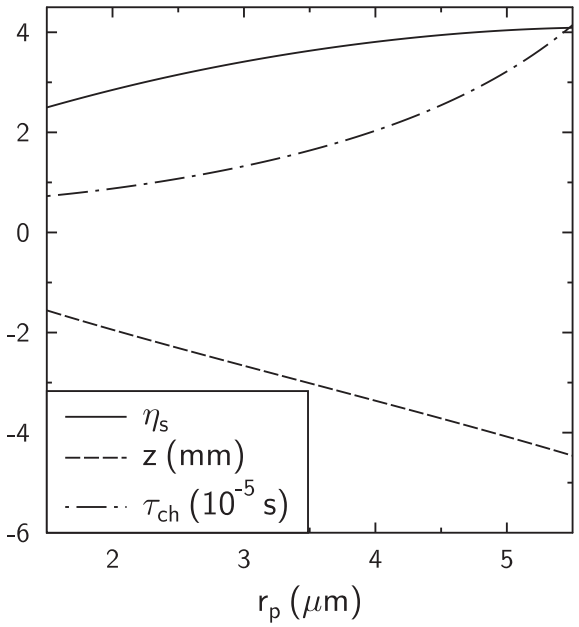

FIG. 4. Normalized surface potential η_s, levitation height z, and lifetime of a charge fluctuation τ_{ch} for SiO_2 particles as a function of the particle radius r_p.

This method works best for small particles, which have large velocities and are not affected by the noise from errors in position measurements. For each of the Brownian particles we determine its proper radius from the Epstein drag. The radius of silica particles is nearly unaffected by the drying process with a radius reduction of $\delta r = -0.02\,\mu$m. It becomes substantial ($\delta r = -0.16\,\mu$m) for MF particles, as shown in the inset of Fig. 3. At last, we obtain the kinetic temperature as $T_k = (m_p/k_B)\langle v^2\rangle$.

Finally, the accuracy of the obtained temperatures needs attention. The determination of particle positions with subpixel resolution from digital images was discussed in Refs. [22,30]. Possible error sources for particle velocities, such as pixel locking, and their influence on kinetic temperatures were described in Ref. [31]. Because of their mostly technical nature, details of our data handling procedure are compiled in the Appendix. The influence of the position error turns out negligible. The typical confidence interval from the bootstrapping analysis extends over ± 5 K.

IV. CHARGE FLUCTUATIONS

A microparticle in a plasma is electrically charged due to the flux of electrons and positive ions that reach the surface. Because of the higher thermal velocity of the electrons the net charge is negative. In collisionless plasmas, the net charge is given by the orbital-motion-limited (OML) model [32,33]. Charge exchange collisions in the quasineutral plasma bulk lead to enhanced ion currents and smaller negative charges [34–36]. Recently, we have proposed a model for charging and charge fluctuations with collision-enhanced ion currents in the sheath [37].

The charge on the microparticle fluctuates because of the graininess of the incoming flux, which represents a Markov process [17,18]. When the particle charge deviates by δq from its equilibrium value, a particle suspended in the sheath experiences a stochastic force $\delta q\,\bar{E}_0$. Typical lifetimes of a charge fluctuation are $(10-40)\,\mu$s (see Fig. 4). Since the lifetime of a charge fluctuation in these low-density plasmas is much greater than the r.f. period, the time-averaged electric field $\bar{E}_0$ is used. The efficiency of stochastic heating increases with the lifetime $\tau_{ch} = \gamma_{ch}^{-1}$ of the charge fluctuation. The charging rate γ_{ch} takes the general form [37]

$$\gamma_{ch} = \frac{eI_i}{C_p k_B T_e} f(v_i, \eta_s)\,. \tag{5}$$

Here, I_i is the ion current arriving at the particle surface, $C_p = 4\pi\epsilon_0 r_p$ the capacitance of the particle and T_e the electron temperature. The function $f(v_i,\eta_s)$ depends on the ion velocity v_i at the levitation position and the normalized surface potential $\eta_s = -e\phi_s/k_B T_e$ and has typical values $f \approx 2.5$–3.5. Details of the function $f(v_i,\eta_s)$ can be found in Ref. [37]. Efficient stochastic heating from charge fluctuations is therefore expected for small ion currents and large electric fields. Therefore, stochastic heating should become prominent for heavy particles that require a large electric field for levitation.

A proper expression for the temperature rise ΔT_k from stochastic heating by charge fluctuations can be obtained as follows: The superposition of classical Brownian motion and stochastic heating by charge fluctuations in a harmonic trap can be described by the stationary Klein-Kramers equation [38]

$$0 = \beta\frac{\partial}{\partial v}(vf) + \left(D_v^A + D_v^Q\right)\frac{\partial^2 f}{\partial v^2} \tag{6}$$

for the velocity distribution $f(v)$ of the Brownian particle. Here, D_v^A and D_v^Q are the diffusion coefficients in velocity space due to atomic collisions and charge fluctuation forces, respectively. The diffusion coefficients can be added because the two processes are uncorrelated. The solution of Eq. (6) is a Maxwellian with kinetic temperature $T_k = (m_p/\beta k_B)(D_v^A + D_v^Q)$. The coefficient $D_v^A = (\beta/m_p)k_B T_g$

TABLE I. Parameters for charging model from XPDP1 simulation.

Particle	p (Pa)	U_{rf} (V_{pp})	T_e (eV)	n_{is} (m^{-3})	v_{i0} ($m\ s^{-1}$)	$\langle n_e\rangle/n_i$
SiO_2	10	80	2.30	3.04×10^{14}	326	0.8
MF	11	70	3.01	2.60×10^{14}	320	0.8

is determined by the gas temperature [38]. The diffusion coefficient in v-space $D_v^Q = D_Q \bar{E}_0^2/(m_p^2\gamma_{ch}^2)$ contains the charge diffusivity in Q-space $D_Q = \gamma_{ch}\sigma_Q^2$ [39] with the charge variance $\sigma_Q^2 \approx 0.5eq_p$ [17,40]. Replacing $\bar{E}_0$ by means of the Millikan condition (1), we obtain the temperature rise

$$\Delta T_k = \frac{\sigma_Q^2 m_p g^2}{k_B \beta \gamma_{ch} q_p^2}\ , \tag{7}$$

which states earlier results more precisely that were obtained by treating the charge fluctuations as bandwidth-limited white noise [9] or by means of the Langevin equation [19]. Equation (7) confirms the expected scaling of the temperature rise $\Delta T_k \propto m_p/(q_p\beta\,\gamma_{ch})$. Note that σ_Q^2/q_p is approximately constant. Therefore, the temperature rise is only determined by m_p/q_p and $(\beta\gamma_{ch})^{-1}$. Both dependencies will be studied experimentally in Sec. VI by varying the particle radius and in Sec. VII by varying the gas pressure.

V. THE CHARGING MODEL

The plasma conditions for gas pressures of $p = (10–11)$ Pa are taken from particle-in-cell (PIC) simulations of the r.f. sheath with the XPDP1 code [41,42]. This one-dimensional code is appropriate for our system as long as the confinement region for the microparticle has an almost stratified structure of equipotentials. In this pressure range the sheath thickness is typically 9 mm and the bulk plasma fills only the central 12 mm of the 30 mm gap between the electrodes. The influence of the manipulation electrode is restricted to the outer part of the sheath and its influence on the bulk plasma and plasma production is weak. For lower gas pressures, however, the sheath region expands even further and the central bulk plasma gradually disappears. Then, the manipulation electrode may affect a larger volume and the overall potential structure needs reexamining in more detail using a two-dimensional simulation code. This extension is beyond the scope of the present investigation.

Although experiments in the pressure regime of about 10 Pa resulted in bi-Maxwellian electron distributions in the plasma center [43], our simulations yield an electron distribution function at the sheath edge that is nearly Maxwellian and represents the hot component of the bi-Maxwellian. The resulting parameters for the charging model in the sheath are compiled in Table I.

The particle charge q_p, ion charging current I_i, and γ_{ch} are described by the model in Ref. [37]. The plasma density n_{i0} at the sheath edge and the ion flux density $n_{i0}v_{i0}$ into the sheath are taken from the simulation. The particle charge and the electric field $\bar{E}_0$ are obtained by simultaneously solving the Millikan condition (1) and the floating condition, $I_i + \langle I_e\rangle = 0$. Due to the periodic sheath expansion and contraction, the period-averaged electron density at the levitation height is only ≈80% of the ion density.

In accordance with the PIC simulations, we assume a linear increase of the time-averaged space charge in the outer parts of the sheath, which results in a square law for the electric field. For the conditions in Table I for silica particles the model calculations yield the normalized surface potential η_s, the levitation height z in the sheath, and the lifetime of a charge fluctuation τ_{ch} as a function of the particle radius.

With increasing particle radius (and mass) the levitation height moves ever deeper into the sheath. Since the levitation field increases with m_p/q_p, the ion Mach number increases accordingly. The increasing Mach number leads to a reduction of the OML current to the grain. This reduction is responsible for the increase of the normalized surface potential η_s and, from Eq. (5) for the increase of the lifetime of a charge fluctuation.

The ion drift velocity at the levitation height, $v_i = (e\bar{E}\lambda/m_i)^{1/2}$ is determined from the ion mobility in a weakly collisional sheath using a constant mean free path of $\lambda = 7.0\,\mathrm{mm}/[p(Pa)]$ [44]. The ion current to the microparticle is then calculated from the OML model. This is justified, because the final deflection of the ion orbit by the microparticle occurs on a distance much shorter than the mean free path. Hence, the increase of the particle cross section is still given by the OML factor, but using the proper local ion drift velocity.

VI. VARIATION OF THE PARTICLE SIZE

We first study the evolution of the kinetic temperature with increasing particle size at gas pressures near 10 Pa, which are typical of many experiments with dust clusters.

The measured kinetic temperatures $T_{k,x}$ and $T_{k,z}$ are shown in Fig. 5 together with the predicted temperature rise from Eq. (7). For both species of particles, the experimental data are

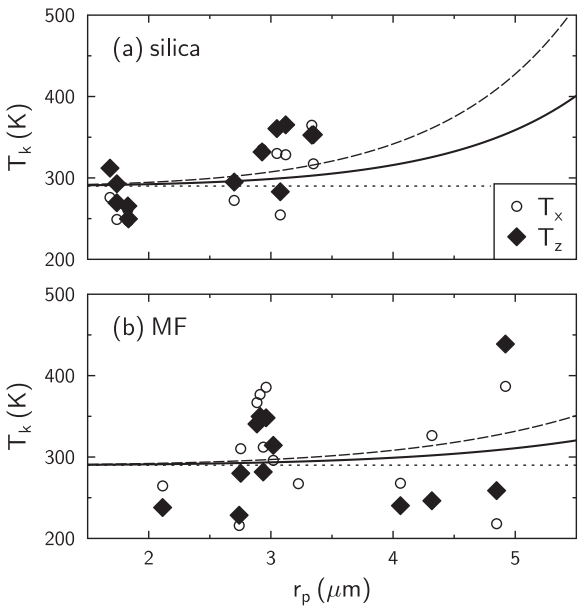

FIG. 5. The measured kinetic temperatures for (a) silica and (b) MF particles in comparison with the predicted temperature rise from charge fluctuations (solid line). The dashed line corresponds to $2 \times \Delta T_k$. The dotted line marks the gas temperature (290 K).

found close to the gas temperature of 290 K, which is marked by a dotted line. We ascribe the scatter of the data points to residual uncertainties of the particle mass. For silica particles we observe a weak rise of the kinetic temperature with particle mass. A similar temperature rise is only found for the largest MF particles. This result is generally in agreement with the expectation that heavier particles require a larger levitation field, which in turn determines the heating rate.

Our heating model that combines the charging model [37] with plasma parameters from PIC simulations gives a reasonable quantitative description of the heating process by charge fluctuations. In particular, we find that the temperature rise with particle size should be small. On average, the experiments indicate a weak trend of such a temperature rise. The observed trend of the experimental data would be even better described by twice the heating rate from Eq. (7) as indicated by the dashed line in Fig. 5. In view of the data scatter no significant difference between $T_{k,x}$ and $T_{k,z}$ can be stated.

VII. PRESSURE VARIATION

A substantial temperature rise can be expected by lowering the gas temperature. The temperature rise predicted by Eq. (7) on the one hand depends on the lifetime of the fluctuations $\tau_{ch} = \gamma_{ch}^{-1}$. From Eq. (5) we see that the charging rate γ_{ch} is proportional to the ion charging current, which is proportional to the plasma density at the sheath edge.

The plasma density in the center of rf-discharges at very low pressures generally shows an erratic dependence on gas pressure [45], which can be attributed to the accumulation of cold electrons in the plasma center.

On the other hand, detailed probe measurements [46] have shown that the density of hot plasma electrons, which are able to penetrate the sheath and determine the dust charge, scales with the gas pressure, $n_i \propto p$. This scaling would already predict a temperature rise for decreasing gas pressure. Moreover, the temperature rise depends also on the cooling rate β. According to the Epstein formula (4) we have a scaling $\beta \propto p$. Combining these two aspects, we expect that the temperature rise at pressure reduction approximately scales as $\Delta T_k \propto p^{-2}$. Therefore, a pressure reduction by a factor of three should roughly give a temperature rise by an order of magnitude.

Since we have learned in the preceding paragraph that the heating is most efficient for the largest particle mass, we use the largest available silica particle size of $r_p = 3.69\,\mu$m. The experiment is made by trapping a single particle at the lowest pressure ($p = 3$ Pa) that provides stable levitation. Then the Brownian motion for this specific particle is recorded at stepwise increasing gas pressure. This procedure eliminates any ambiguity in the particle radius. Further, we have learned before that the silica particle ensures long-time stability.

The resulting kinetic temperatures $T_{k,z}$ are compiled in Fig. 6(a). The error bars represent an uncertainty of 10%. As a guide to the eye, the estimated temperature rise $\propto p^{-2}$ is shown by the solid curve. The observed temperature rise generally confirms the expected scaling from the combined influence of extended lifetime of a fluctuation and reduced cooling rate when the pressure is lowered.

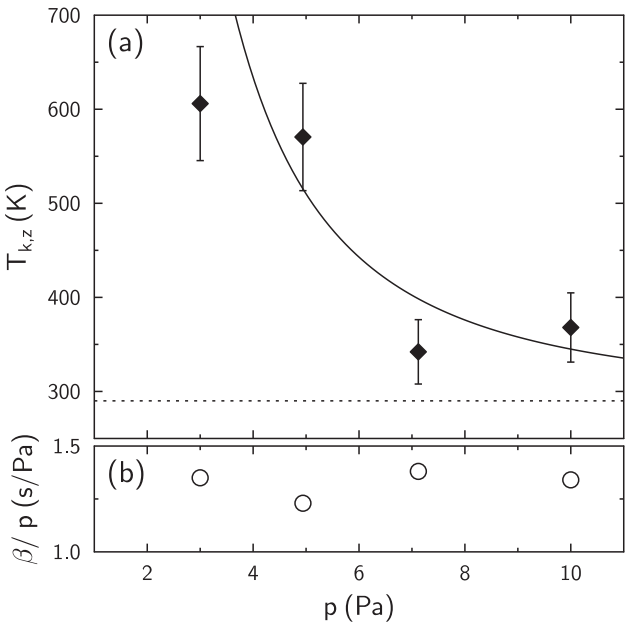

FIG. 6. (a) The measured kinetic temperature $T_{k,z}$ for a silica particle of 3.69 μm radius. The full curve indicates the estimated p^{-2} scaling. The dotted line marks the gas temperature (290 K). (b) The normalized friction coefficient β/p as obtained from the VAF.

The Epstein friction β obtained from the VAF is used on the one hand to verify the pressure scaling $\beta \propto p$. On the other hand, deviations from this scaling could be taken as an indication for a competing instability, which may also be a source of heating. The normalized friction coefficient β/p in Fig. 6(b) shows no significant dependence on the gas pressure. This confirms the Epstein formula and rules out any substantial reduction of the friction coefficient by instabilities, such as the delayed charging instability [47].

VIII. DISCUSSION

The experimental techniques have been thoroughly refined to make precise measurement of kinetic temperatures near room temperature accessible. Since the kinetic temperature is the product of the mean-squared velocity and the particle mass, we have applied a proper determination of particle velocities in the ballistic regime. Further, the particle mass was determined from precise values of the Epstein friction coefficient obtained from the VAF. The position error was found to have a negligible influence on the kinetic temperature. In this way we could clearly demonstrate that for a gas pressure of the order of 10 Pa the kinetic temperature of an isolated silica particle remains close to gas temperature. For MF particles the substantial corrections from the Epstein drag lead to consistent temperatures. In this way, we can conclude that excessive temperatures reported at these plasma conditions for many-particle systems can be attributed to collective instabilities.

We have presented a detailed heating model that is based on reliable plasma parameters from PIC simulations and contains no fit parameters. This model allows for an absolute comparison between theory and experimental data. In the

accessible range of particle sizes and at 10 Pa pressure, the predicted heating effect from charge fluctuations is as small as the experiments show. On average, a weak trend of temperature rise with increasing particle mass becomes visible in the experimental data, although the remaining scatter is of the same order as the temperature increase.

A pronounced heating effect, however, is found when the gas pressure is reduced. Pressure reduction increases the lifetime of a fluctuation and reduces the cooling rate. Since both aspects act simultaneously, a general scaling $\Delta T \propto p^{-2}$ was expected and could be generally confirmed by the experimental data. For a refined analysis, the scaling of the plasma parameters with gas pressure need to be determined. This remains a challenging task, because PIC simulations with a two-dimensional code will be necessary that describe the sheath region including the distortion by the manipulation electrode. Detailed experiments and comparative simulations will be the subject of future investigations.

During pressure reduction the normalized friction coefficient β/p remained constant as expected from Epstein's formula. This finding rules out any competing instability, such as the delayed charging instability [47] that was observed by other authors at pressures $p < 2$ Pa. Such an instability would otherwise manifest itself by a gradual reduction of the damping rate even before the instability sets in.

The experiments with single Brownian particles have excluded all collective heating mechanisms. In this way we could show that the motion of the microparticle under the sole influence of classical Brownian motion in the gas and white noise from charge fluctuation forces leads to a Maxwellian velocity distributions at a slightly enhanced temperature, mean square displacements and velocity autocorrelations in close agreement with the Uhlenbeck-Ornstein-Wang model [26,27].

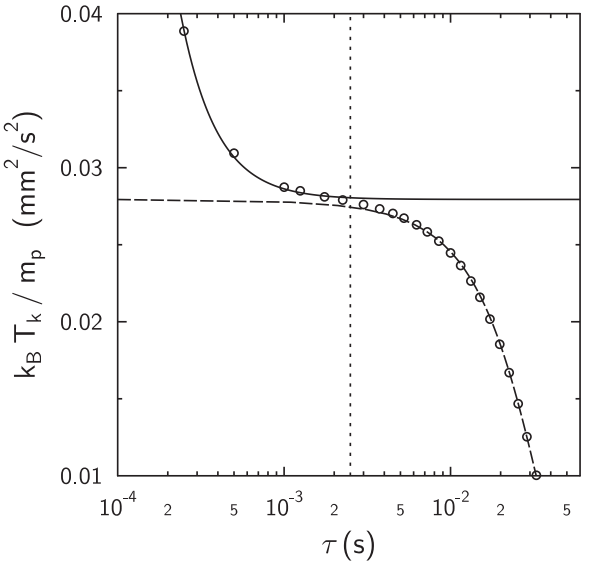

FIG. 7. Resulting kinetic temperatures as a function of the chosen time step τ. The dashed line represents the transition from the diffusive to ballistic regime given by the Uhlenbeck-Ornstein model, which approaches T_k^{true} for $\tau \to 0$. The solid line is the error model from Eq. (A1). The vertical dotted line marks the standard sampling rate of $f_s = 400$ fps.

The topic of Brownian motion under the influence of additional stochastic heating from charge fluctuations will continue to be an interesting topic, because it is a particular situation, in which the second stochastic process introduces fluctuations but no damping. Stochastic heating by charge fluctuations cannot be interpreted as a second heat bath, as was the case in hot Brownian motion. Rather, we have shown above that the superposition of a stochastic process without damping can be correctly described by the Klein-Kramers equation (6), which allows a quantitative prediction of the temperature rise (7).

ACKNOWLEDGMENTS

The authors thank Dietmar Block for helpful comments on the manuscript and Franko Greiner for discussions on the PIC simulations. This work was supported by DFG within the Transregional Collaborative Research Centre TR-24, "Fundamentals of Complex Plasmas", project A2.

APPENDIX: EXPERIMENTAL ERRORS AFFECTING THE KINETIC TEMPERATURE

Particle velocities result from the difference Δr of positions at a chosen time step τ. When the time step is chosen too small, the resulting velocity $v = \Delta r/\tau$ is affected by the error σ_r of the position measurement and asymptotically approaches

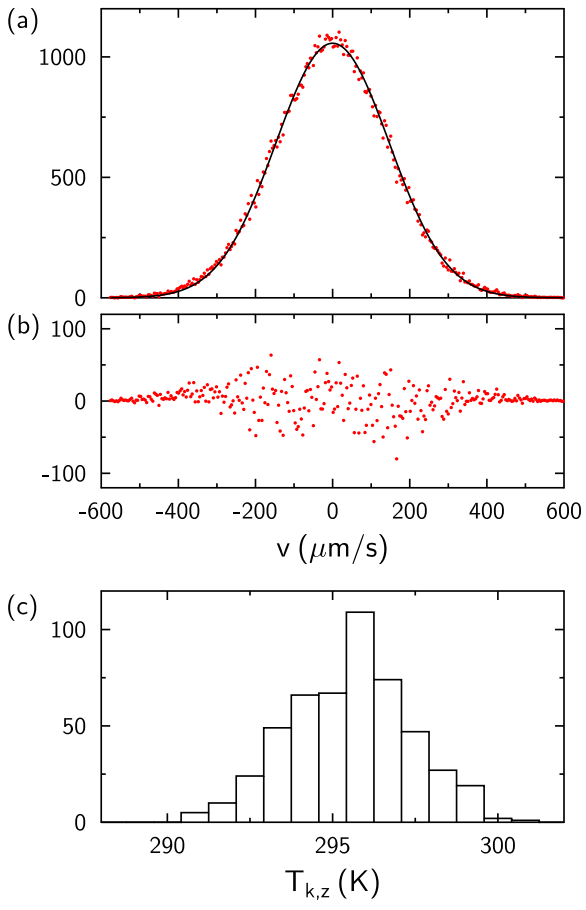

FIG. 8. (Color online) (a) The velocity distribution function $f(v_z)$ from the data used in the inset of Fig. 2. The full line gives the best fit, (b) residue of this fit, (c) temperature distribution from the bootstrap analysis.

spurious velocities $v = 2^{1/2}\sigma_r/\tau$ [31]. On the other hand, a too large time step leads to apparently reduced temperatures by leaving the ballistic regime. The optimum choice for τ can be obtained from a high-speed recording with a sampling rate of $f_s = 4000$ fps. In this time series the time step for evaluating the velocity $\tau = N/f_s$ is varied by skipping an increasing number N of frames [31]. The resulting kinetic temperatures are plotted vs. τ in Fig. 7.

The data points show the expected increase $\propto\tau^{-2}$ below the inflection point. Above the inflection point, the kinetic temperature decreases as expected from the Uhlenbeck-Ornstein model. The dashed curve is a fit based on Eq. (2) to these data, which approaches T_k^{true} for $\tau \to 0$. The position error σ_r in this measurement can be extracted by fitting the temperatures below the inflection point by an error model (solid line in Fig. 7) that describes the deviation from the true kinetic temperature T_k^{true}

$$T_k = T_k^{\text{true}} + \frac{m_p}{N_s k_B}\frac{2\sigma_r^2}{\tau^2}\,. \tag{A1}$$

Here $N_s = 10^4$ is the sample size of individual velocity measurements in this time series at $N = 10$ skipped frames and the individual errors are assumed to follow Poisson statistics. This fit yields $\sigma_r = 1.9\,\mu$m. Compared to the effective pixel size of $7\,\mu$m in real space coordinates we achieve a subpixel resolution of about 1/4 pixel.

As optimum choice for T_k we could use the value at the inflection point of this curve. However, this information is only available after an elaborate data analysis. For practical reasons, we have therefore chosen a fixed predetermined sampling rate $f_s = 400$ fps, which lies in the plateau close to the inflection point. Accordingly, we neglect the small correction originating from using $T_k(400\text{ fps})$ instead of T_k^{true} in this paper.

Besides these systematic error sources, the statistical error in fitting the measured distribution function by a Gaussian can be estimated by "bootstrapping" [48]. Confidence limits are obtained by taking the residue of the fit as an estimate for the statistical error. This is done by adding randomized errors taken from this residue to the best-fit Maxwellian and repeating the fitting procedure 500 times. In Fig. 8(a) the best fit Maxwellian $f(v_z)$ is shown for the same data as in the inset of Fig. 2 together with (b) the residue and (c) the temperature distribution from the bootstrap analysis.

The confidence interval, which contains 95% of the bootstrapped temperature values, extends over ± 5 K. This statistical error is much smaller than the observed scatter of the measured temperatures in Fig. 5, which hints at additional still unidentified error sources.

[1] T. C. Li, S. Kheifets, D. Medellin, and M. G. Raizen, Science **328**, 1673 (2010).
[2] R. X. Huang, I. Chavez, K. M. Taute, B. Lukić, S. Jeney, M. G. Raizen, and E.-L. Florin, Nat. Phys. **7**, 576 (2011).
[3] S. Kheifets, A. Simha, K. Melin, T. Li, and M. G. Raizen, Science **343**, 1493 (2014).
[4] D. Rings, R. Schachoff, M. Selmke, F. Cichos, and K. Kroy, Phys. Rev. Lett. **105**, 090604 (2010).
[5] J. Millen, T. Deesuwan, P. Barker, and J. Anders, Nat. Nanotechnol. **9**, 425 (2014).
[6] G. Falasco, M. V. Gnann, D. Rings, and K. Kroy, Phys. Rev. E **90**, 032131 (2014).
[7] J. Williams and E. Thomas, Jr., Phys. Plasmas **13**, 063509 (2006).
[8] A. Melzer, A. Homann, and A. Piel, Phys. Rev. E **53**, 2757 (1996).
[9] R. A. Quinn and J. Goree, Phys. Rev. E **61**, 3033 (2000).
[10] S. Nunomura, J. Goree, S. Hu, X. Wang, and A. Bhattacharjee, Phys. Rev. E **65**, 066402 (2002).
[11] A. Melzer, Phys. Rev. E **67**, 016411 (2003).
[12] A. K. Mukhopadhyay and J. Goree, Phys. Rev. Lett. **109**, 165003 (2012).
[13] A. K. Mukhopadhyay and J. Goree, Phys. Rev. Lett. **111**, 139902(E) (2013).
[14] V. A. Schweigert, I. V. Schweigert, A. Melzer, A. Homann, and A. Piel, Phys. Rev. E **54**, 4155 (1996).
[15] L. Couedel, V. Nosenko, A. V. Ivlev, S. K. Zhdanov, H. M. Thomas, and G. E. Morfill, Phys. Rev. Lett. **104**, 195001 (2010).
[16] A. Melzer, Phys. Rev. E **90**, 053103 (2014).
[17] C. Cui and J. Goree, IEEE Trans. Plasma Sci. **22**, 151 (1994).
[18] T. Matsoukas, M. Russell, and M. Smith, J. Vac. Sci. Technol. A **14**, 624 (1996).
[19] O. S. Vaulina, S. A. Khrapak, A. P. Nefedov, and O. F. Petrov, Phys. Rev. E **60**, 5959 (1999).
[20] A. Melzer, T. Trottenberg, and A. Piel, Phys. Lett. A **191**, 301 (1994).
[21] C. Schmidt, O. Arp, M. Himpel, A. Melzer, and A. Piel, IEEE Trans. Plasma Sci. **41**, 774 (2013).
[22] Y. Ivanov and A. Melzer, Rev. Sci. Instrum. **78**, 033506 (2007).
[23] Microparticles GmbH, Berlin, Germany.
[24] J. Carstensen, H. Jung, F. Greiner, and A. Piel, Phys. Plasmas. **18**, 033701 (2011).
[25] C. Killer, M. Mulsow, and A. Melzer, Plasma Sources Sci. Technol. **24**, 025029 (2015).
[26] G. E. Uhlenbeck and L. S. Ornstein, Phys. Rev. **36**, 823 (1930).
[27] M. C. Wang and G. E. Uhlenbeck, Rev. Mod. Phys. **17**, 323 (1945).
[28] P. Epstein, Phys. Rev. **23**, 710 (1924).
[29] H. Jung, F. Greiner, O. H. Asnaz, and A. Piel, Phys. Plasmas **22**, 053702 (2015).
[30] Y. Feng, J. Goree, and B. Liu, Rev. Sci. Instrum. **78**, 053704 (2007).
[31] Y. Feng, J. Goree, and B. Liu, Rev. Sci. Instrum. **82**, 053707 (2011).
[32] J. E. Allen, Phys. Scr. **45**, 497 (1992).
[33] T. Nitter, Plasma Sources Sci. Technol. **5**, 93 (1996).
[34] M. Lampe, R. Goswami, Z. Sternovsky, S. Robertson, V. Gavrishchaka, and G. Ganguli, Phys. Plasmas **10**, 1500 (2003).
[35] S. A. Khrapak, S. V. Ratynskaia, A. V. Zobnin, A. D. Usachev, V. V. Yaroshenko, M. H. Thoma, M. Kretschmer, H. Höfner, G. E. Morfill, O. F. Petrov, and V. E. Fortov, Phys. Rev. E **72**, 016406 (2005).
[36] I. H. Hutchinson and L. Patacchini, Phys. Plasmas **14**, 013505 (2007).

[37] A. Piel and C. Schmidt, Phys. Plasmas **22**, 053701 (2015).
[38] H. Risken, *The Fokker-Planck Equation* (Springer, Berlin, 1984).
[39] T. Matsoukas and M. Russell, Phys. Rev. E **55**, 991 (1997).
[40] T. Matsoukas and M. Russell, J. Appl. Phys. **77**, 4285 (1995).
[41] J. P. Verboncoeur, M. V. Alves, V. Vahedi, and C. K. Birdsall, J. Comp. Phys. **104**, 321 (1993).
[42] V. Vahedi, G. DiPeso, C. K. Birdsall, M. A. Liebermann, G. DiPeso, and T. D. Rognlien, Plasma Sources Sci. Technol. **2**, 261 (1993).
[43] V. A. Godyak, R. B. Piejak, and B. M. Alexandrovich, Plasma Sources Sci. Technol. **1**, 36 (1992).
[44] A. V. Phelps, J. Phys. Chem. Ref. Data **20**, 557 (1991).
[45] V. Vahedi, C. K. Birdsall, M. A. Liebermann, G. DiPeso, and T. D. Rognlien, Plasma Sources Sci. Technol. **2**, 273 (1993).
[46] V. A. Godyak, R. B. Piejak, and B. M. Alexandrovich, J. Appl. Phys. **73**, 3657 (1993).
[47] S. Nunomura, T. Misawa, N. Ohno, and S. Takamura, Phys. Rev. Lett. **83**, 1970 (1999).
[48] W. H. Press, B. P. Flannery, S. A. Teukolsky, and W. T. Vetterling, *Numerical Recipes*, 3rd ed. (Cambridge University Press, Cambridge, UK, 2007).